ACS OMEGA

http://pubs.acs.org/journal/acsodf

Article

Neat Protein Single-Chain Nanoparticles from Partially Denatured BSA

Paula Malo de Molina,* Thu Phuong Le, Amaia Iturrospe, Urs Gasser, Arantxa Arbe, Juan Colmenero, and José A. Pomposo

Cite This: *ACS Omega* 2022, 7, 42163−42169

Read Online

ACCESS | Metrics & More | Article Recommendations | Supporting Information

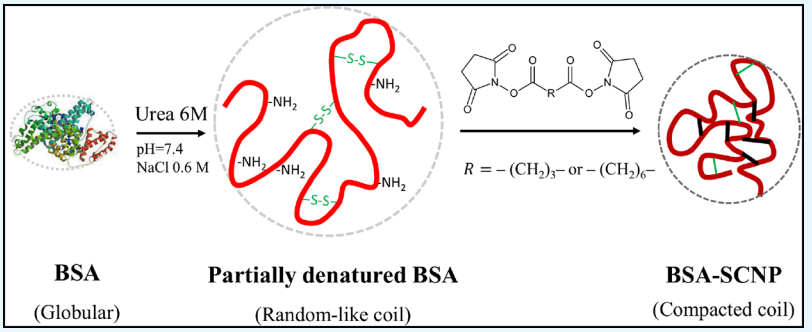

ABSTRACT: The main challenge for the preparation of protein single-chain nanoparticles (SCNPs) is the natural complexity of these macromolecules. Herein, we report the suitable conditions to produce "neat" bovine serum albumin (BSA) single-chain nanoparticles (SCNPs) from partially denatured BSA, which involves denaturation in urea and intramolecular cross-linking below the overlap concentration. We use two disuccinimide ester linkers containing three and six methylene spacer groups: disuccinimidyl glutarate (DSG) and disuccinimidyl suberate (DSS), respectively. Remarkably, the degree of internal cross-linking can be followed simply and efficiently via ^{1}H NMR spectroscopy. The associated structural changes—as probed by small-angle neutron scattering (SANS)—reveal that the denatured protein has a random-like coil conformation, which progressively shrinks with the addition of DSG or DSS, thus allowing for size control of the BSA-SCNPs with radii of gyration down to 5.4 nm. The longer cross-linker exhibits slightly more efficiency in chain compaction with a somewhat stronger size reduction but similar reactivity at a given cross-linker concentration. This reliable method is applicable to a wide range of compact proteins since most proteins have appropriate reactive amino acids and denature in urea. Critically, this work paves the way to the synthesis of "neat", biodegradable protein SCNPs for a range of applications including nanomedicine.

1. INTRODUCTION

Single-chain nanoparticles (SCNPs) are discrete polymer chains folded or collapsed via intramolecular cross-linking under dilute conditions. Due to their small size, softness, and internal compartmentalization, they have potential applications in catalysis, sensing, and drug delivery[1] as well as in all-polymer nanocomposites.[2,3] Up to date, most efforts have been focused on SCNPs obtained from synthetic macromolecules. More recently, there has been great interest in expanding this technology to biodegradable and biocompatible polymers,[4] including proteins.[5]

Numerous synthesis strategies of SCNPs from synthetic (co)polymers have been reported, which typically involve two steps: functionalization of a linear precursor and subsequent internal cross-linking.[6] Each cross-link between two reactive functional sites of the chain generates an internal loop, and globally, the precursor chain reduces its size. The resulting shrinking can be monitored by experimental techniques of different degrees of complexity, e.g., size exclusion chromatography (SEC) and dynamic light scattering (DLS).[7] These are indirect methods that have shown that the length and flexibility of the cross-linker have a significant impact in the chain folding.[8,9] However, changes in the polymer conformation, i.e., an increase in internal particle compactness that goes along with the size reduction, are best probed directly with small angle X-ray scattering (SAXS) or small angle neutron scattering (SANS) techniques, thanks to the scattering vector (Q) dependence of the measured intensities.[10] Direct structural determination by SAXS/SANS with the aid of simulations and scaling analysis has shown that the usual

Received: July 29, 2022
Accepted: October 26, 2022
Published: November 9, 2022

morphology of SCNPs is sparse with internal loops that leads to the presence of local "pockets".[11] Furthermore, unlike globular proteins whose folding is given by defined interactions, the collapse of synthetic SCNPs is the result of a stochastic process leading not only to a less controlled compaction but also to a polydispersity of resulting topologies.[12,13]

In addition to their applications as soft synthetic nanoparticles, synthetic SCNPs are considered as simple models to mimic the more compositionally complex intrinsically disordered proteins (IDPs).[14] The main advantage of synthetic SCNPs as IDP models is their simpler chemical composition, which makes it possible to isolate excluded volume effects particularly relevant in crowded environments.[14] However, real proteins are compositionally more complex due to the chemical diversity of the proteinogenic amino acids. Thus, the synthesis of polypeptide single-chain nanoparticles bridges the gap between synthetic SCNPs and proteins, thereby extending their potential applications. In particular, protein SCNPs could find interest in nanomedicine, where gene therapy is its largest emergent field.[15]

To synthesize "neat" protein-based SCNPs, we chose the protein BSA (bovine serum albumin) because it has several advantages as a precursor. First, it consists of a well-characterized long polypeptide single chain with approximately 10% of reactive lysine residues homogeneously distributed along the chain that are available for cross-linking. Furthermore, globular BSA denatures in the presence of chemical denaturants such as urea and adopts a random-like coil conformation.[16] Urea denatures proteins by breaking the H-bonds and by increasing the solvation of hydrophobic groups.[17] Last but not least, serum albumins, due to their availability, low cost, and low immunogenicity, are great candidates for the synthesis of nanoparticles. In fact, protein nanoparticles with radii ranging from tens to hundreds of nanometers have been made from BSA for applications in targeted drug delivery and pH sensing.[18,19] In this article, we report a procedure to push down the size to that of a neat polypeptide single chain. In a recent work, "hybrid" SCNPs of human serum albumin stabilized with PEG grafts were synthesized with a hydrodynamic radius of down to 9.5 nm.[5] Here, we show that it is possible to obtain "neat" SCNPs from unPEGylated BSA with radius of gyration of down to 5.4 nm. With this aim, we have adopted the strategy to cross-link internally the lysine residues of denatured BSA using two cross-linkers of different lengths: disuccinimidyl suberate (DSS) and disuccinimidyl glutarate (DSG) (see Figure 1,A,B) and exploited our previous experience in the preparation and characterization of synthetic unimolecular SCNPs.[6]

2. MATERIALS AND METHODS

2.1. Materials. Bovine serum albumin (BSA), disuccinimidyl glutarate (DSG), urea, sodium chloride (NaCl), phosphate-buffered saline (PBS, powder, pH 7.4, for preparing 1 L solutions), and dimethyl sulfoxide were obtained from Sigma-Aldrich. Disuccinimidyl suberate (DSS) was purchased from Acros Organics. Deionized water was obtained from a Thermo Scientific apparatus (Barnstead TII Pure Water System). Deuterium oxide (D_2O, 99.9% D), deuterated urea (D4, 98% D), and deuterated dimethyl sulfoxide (d_6-DMSO, 99.8% D) were obtained from Eurisotop and used without further purification. Deuterated PBS (*d*-PBS) powder was prepared from hydrogenated PBS powder by exchanging the hydrogen atoms for deuterium, dissolving the salts in D_2O, followed by freeze-drying. Similarly, the BSA for SANS was dissolved in D_2O to remove exchangeable protons, and after 1 day of incubation, the solution was lyophilized. This process was performed twice.

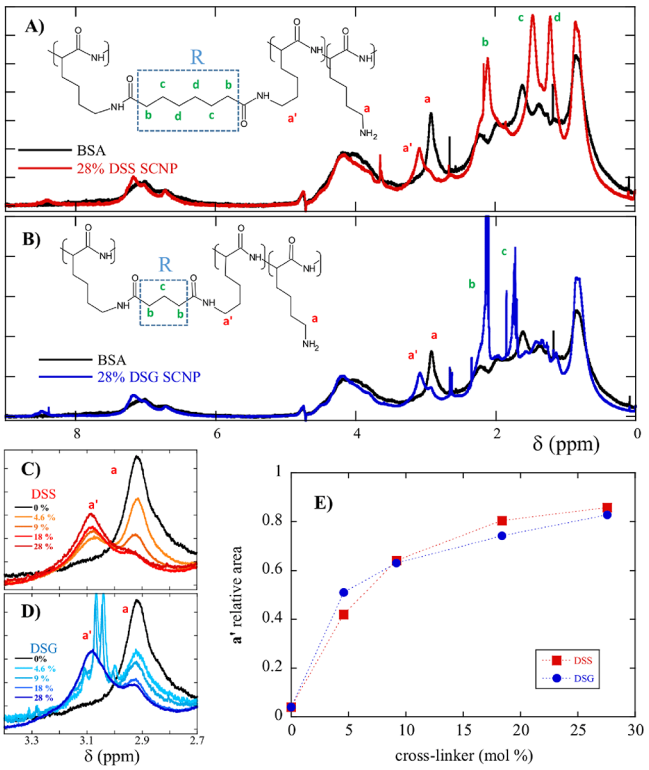

Figure 1. ^{1}H-NMR spectra of BSA (black line) and BSA-SCNPs with (A) 28 mol % DSS (red line) and (B) 28 mol % DSG (deep blue line). The inset shows the chemical structure of a cross-link between two lysine groups. (C, D) Zoom of the peaks **a** and **a′** for all BSA-SCNPs of Table 1 with (C) DSS and (D) DSG cross-linkers. (E) Relative contribution of peak **a′** in (C) and (D) for BSA-SCNPs intramolecularly cross-linked with DSS (red squares) or DSG (blue circles).

2.2. Sample Preparation and BSA-SCNP Formation. Denatured BSA solutions were prepared by mixing 10 vol % of a solution of BSA (10 mg/mL) in PBS and 90 vol % of a solution of urea (6.67 M) and NaCl (0.57 M) in PBS. The final composition thus was BSA (1 mg/mL), urea (6 M), and NaCl (0.6 M) at pH 7.4. BSA-SCNPs were formed by the addition of cross-linker in DMSO (with concentrations of 5−8 wt %) and stirred for at least 12 h. SANS samples were prepared with partially hydrogenated BSA, hydrogenated cross-linkers in deuterated DMSO, deuterated urea, *d*-PBS, and D_2O. The structural characterization with SANS and SAXS (see the SI) was performed directly in the reacting medium. Samples for ^{1}H-NMR were dialyzed against decreasing concentrations of urea until the proteins were in water and subsequently dialyzed against water. Then, the protein SCNPs were lyophilized and redissolved in D_2O.

^{1}H nuclear magnetic resonance (^{1}H NMR) spectra were recorded at room temperature on a Bruker spectrometer operating at 400 MHz using D_2O as solvent. The solution density was measured with a DMA 4500 M apparatus from Anton Paar. The pH was measured with a Laquatwin pH meter from Horiba.

https://doi.org/10.1021/acsomega.2c04805
ACS Omega 2022, 7, 42163−42169

Table 1. Summary of the Main Properties of Native BSA, (Partially) Denatured BSA, and BSA-SCNPs as Determined by ^{1}H NMR and SANS Measurements

sample	cross-linker spacer, R	cross-linker(mol %)[a]	app. lysine conversion(%)[b]	$I(0)^c$ (cm^{-1},±0.003)	$R_g{}^c$(nm)	ν^c(±0.01)
native BSA				0.073	3.7 ± 0.1[d]	
denatured BSA				0.106	7.38 ± 0.2	0.50
SCNP #1	$(CH_2)_3$	4.6	51	0.109	6.65 ± 0.5	0.45
SCNP #2		9.1	63	0.100	6.50 ± 0.6	0.43
SCNP #3		18	74	0.107	5.86 ± 0.3	0.42
SCNP #4		28	83	0.102	5.46 ± 0.3	0.39
SCNP #5	$(CH_2)_6$	4.6	42	0.122	6.07 ± 0.2	0.47
SCNP #6		9.1	64	0.146	6.09 ± 0.4	0.46
SCNP #7		18	80	0.141	5.51 ± 0.5	0.40
SCNP #8		28	86	0.142	5.42 ± 0.3	0.43

[a]Mole percent of cross-linker with respect to the total concentration of protein residues. [b]Relative contribution of peak **a′** from ^{1}H-NMR (see the SI). [c]Parameters obtained from fitting the SANS data with a generalized Gaussian random coil form factor (see eq 3 in the text). [d]The BSA in its native conformation has the form of a prolate ellipsoid with a polar axis of R_p = 7.3 nm and an equatorial axis of R_e = 2.5 nm, with a corresponding radius of gyration of R_g = 3.7 nm (see the SI).

2.3. Small-Angle Neutron Scattering. Small-angle neutron scattering (SANS) measurements were performed on the SANS-I instrument at the Swiss Spallation Neutron Source, SINQ, Paul Scherrer Institut, Switzerland.[20] The mean wavelength of the incident neutron beam was λ= 5 Å with a wavelength resolution of approximately 10% at two sample-to-detector distances of 4.5 and 18 m, respectively, to cover the data in the wave vector transfer Q range of 0.03 to 0.23 nm^{-1}, with $Q = 4\pi\sin(\theta/2)/\lambda$, where θ is the scattering angle. Samples were measured in Quartz Hellma cells (110-QS) of 2 mm thickness. The measured SANS data were corrected and normalized to a cross-sectional unit using BERSANS-PC data processing software.[21] Solvent backgrounds (*d*-PBS in D_2O and *d*-PBS, NaCl, and *d*-urea (6 M) in D_2O) were measured in the same cells and subtracted from the data. The background-corrected scattering curves were fitted to an ellipsoid in the case of BSA in its native conformation and, in the case of BSA and the SCNPs, in denaturing conditions with a model for generalized Gaussian coils.

3. RESULTS AND DISCUSSION

To synthesize neat BSA-SCNPs, we first denatured the protein in phosphate-buffered saline (PBS) with NaCl (0.6 M) and urea (6 M). We used a low protein concentration of 1 mg/mL well below the overlap concentration to avoid, as far as possible, intermolecular cross-linking events. We synthesized the BSA-SCNPs via addition of the cross-linkers DSS and DSG at 0−28 mol % with respect to the total protein aminoacid monomer concentration. DSS and DSG react mainly with the lysine primary amine groups, leading to amide formation as shown in Figure 1A,B. Table 1 collects the library of prepared BSA-SCNPs and their main properties.

First, we examine the cross-linking reaction via ^{1}H-NMR. Figure 1 shows the representative ^{1}H-NMR spectra of the BSA-SCNPs with both cross-linkers compared to that of BSA. As expected in the case of high-molecular weight proteins, the ^{1}H-NMR spectrum of globular BSA is complex since the most part of the protons give rise to broad unresolved resonances.[22] Nevertheless, the main signatures due to cross-linking are visible. First, we observe changes in the chemical shift of the lysine **a** protons corresponding to the change from being linked to a primary amine to being bonded to an amide: disappearance of the peak **a** at 2.92 ppm and appearance of a new peak **a′** at 3.09 ppm (see Figure 1C,D). This shift is much clearer in the cross-linking of poly-lysine where there is no interference of neighbor signals, confirming the peak assignment (see the Supporting Information (SI), Figure S1). In the case of BSA, that peak corresponds to a superposition of the lysine ε- and arginine γ-protons,[22] where in this case, only the lysine is expected to react with succinimide esters and thus contribute to a change in chemical shift. In addition, we observe the emergence of the peaks corresponding to the cross-linker protons **b**, **c**, and **d** for DSS (Figure 1A) and **b** and **c** for DSG (Figure 1B). Finally, some changes in the signal at around 7 ppm, corresponding mainly to thyrosine residues,[22] are also apparent. It is worth mentioning that in addition to the primary amino groups, succinimide ester linkers react to some extent with serine, threonine, and tyrosine.[23] Thus, cross-linking between monomers other than lysine cannot be discarded.

A semi-quantitative estimation of the lysine conversion was made by decomposition and integration of the **a** and **a′** peaks at 2.92 and 3.09 ppm (see the SI, Figure S2). Figure 1E shows the increase of the relative contribution of peak **a′** as a function of the cross-linker amount. The apparent degree of lysine reaction increases as the amount of cross-linker increases until it reaches a point where it plateaus at a maximum value of about 85% because of the contribution of unreactive arginine protons to the signal. The degree of cross-linking of the lysine residues appears to be very similar for both cross-linkers. We also note that the signal corresponding to the protons from the succinimide end-groups (expected to appear around 2.6 ppm; see the SI, Figure S1) is not very significant, indicating that there are not many pendant reactive groups (within the uncertainty of the ^{1}H-NMR technique). It has been shown that the percentage of unreacted cross-linking depends on the polymer conformation, backbone stiffness, and solvent conditions.[24]

The cross-linking reaction described above, when it happens mainly intramolecularly, should lead to a macromolecular size reduction and internal compaction. To probe the structural changes upon protein denaturalization and subsequent SCNP formation, we performed small-angle neutron scattering (SANS) measurements. The scattering contrast was maximized by measuring hydrogenated BSA in solutions with deuterated water and deuterated urea. Figure 2A,B shows the scattering curves of native BSA in PBS solution compared to the denatured state and the BSA-SCNP with 28 mol % DSG both

https://doi.org/10.1021/acsomega.2c04805
ACS Omega 2022, 7, 42163−42169

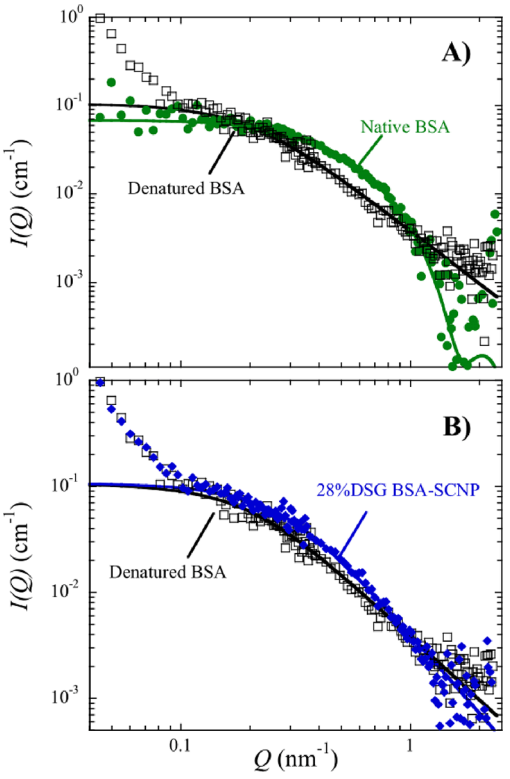

Figure 2. SANS data of (partially) denatured BSA (black squares), native globular BSA (green circles) (A), and internally cross-linked BSA (blue diamonds) (B).

in *d*-urea (6 M)/NaCl (0.6 M)/D_2O. Figure 2A shows that the scattering pattern of the native protein in buffer solution corresponds to rather small and compact objects, whereas denaturation leads to larger objects as seen from the shift of the curve toward lower Q values and the decrease of the intensity decay slope at higher Qs, related to lower degrees of compactness within the object.

In general, the SANS intensity is expressed as[25]

$$I(Q) = \phi \Delta\rho^2 V_p P(Q) S(Q) \quad (1)$$

where ϕ is the protein volume fraction, V_p is the volume of the scattering objects, $\Delta\rho^2$ is the neutron contrast factor, $P(Q)$ is the single particle form factor, and $S(Q)$ is the interparticle structure factor. The neutron contrast is obtained from the difference between the scattering length density (SLD) of the macromolecule and the medium in which it is suspended. The calculated scattering length densities of all compounds are listed in Table S1.

The single-particle form factor of BSA in its native conformation can be described by a model of prolate ellipsoids.[16] The form factor for an ellipsoid with principal axis R_p and equatorial axis R_e is

$$P(Q) = \int_0^1 \left[3\frac{\sin u - u\cdot\cos u}{u^3}\right]^2 d\mu \quad (2)$$

$$u = Q(R_p^2\mu^2 + R_e^2(1-\mu^2))^{1/2}$$

If $R_p > R_e$, the spheroid is a prolate. The volume is $V_p = \frac{4}{3}\pi R_e^2 R_p$. In this analysis, we are dealing with a solution with low protein concentration and relatively high salt concentration, so we assume that the interparticle interactions are negligible and $S(Q) \approx 1$.

The fit agrees well with the experimental data (see Figure 2A) and gives values of R_p = 7.3 nm and R_e = 2.51 nm in good agreement with those found in ref 16. The radius of gyration of a prolate spheroid is $R_g = \sqrt{(2R_e^2 + R_p^2)/5} = 3.63$nm. Even though this is a simplification of the form of the native BSA protein, it demonstrably works well for the description of SANS data and provides the overall dimensions of the particle.[16] Figure S3 shows that the scattering pattern is incompatible with the form factor for a sphere. In addition, the radius of gyration of the BSA in its native conformation was estimated by means of the Guinier approximation at low Q as $I(Q) = I(0)\exp(-R_g^2Q^2/3)$, yielding a value of 3.7 nm (see Figure S3) , in very good agreement with the value obtained with the ellipsoid form factor.

On the other hand, in the presence of urea 6 M, the scattering profile of BSA changes as a consequence of the protein unfolding (see Figure 2A). For the analysis of the denatured BSA we used a generalized Gaussian coil expression[26]

$$I(Q) = I(0)\left[\frac{1}{\nu U^{1/2\nu}}\gamma\left(\frac{1}{2\nu}, U\right) - \frac{1}{\nu U^{1/\nu}}\gamma\left(\frac{1}{\nu}, U\right)\right] \quad (3)$$

where $U = (2\nu+1)(2\nu+2)Q^2R_g^2/6$ and $\gamma(a, x) = \int_0^x t^{a-1}\exp(-t)dt$. This function allows taking into account different compaction degrees of the coil and excluded volume effects. In eq 3, R_g is the radius of gyration and ν is the scaling exponent, which defines the relation between the polymer molar mass and its size $R_g \approx M_W^{\nu}$. ν is 0.5 for an unordered polymer (which is the conformation of a linear polymer chain in θ-conditions), 0.6 for a swollen chain in a good solvent (the so-called self-avoiding-walk conformation), and 1/3 for a polymeric chain collapsed into a globule. Thus, the degree of compaction of the polypeptide chain is characterized through the scaling factor, ν, which determines the Q-dependence of the scattered intensity at intermediate and high Q-values. The forward scattering, $I(0) = \phi\Delta\rho^2V_pS(0)$, contains information on the macromolecular volume $V_p \approx M_W/(N_{AV}d)$ (with M_W as the molecular weight, N_{AV} as the Avogadro number, and d as the mass density).

Equation 3 fits well the data of the denatured BSA with a radius of gyration of R_g = 7.38 nm and a scaling exponent of $\nu \approx 0.5$. Thus, the chain has clearly expanded with respect to the native conformation. The scattering pattern of the BSA-SCNP synthesized with 28 mol % DSG depicted in Figure 2B shows a size reduction with respect to denatured BSA visible in a shift of the scattering pattern toward higher Q-values. The size reduction is confirmed by the fit of the experimental data using eq 3 with R_g = 5.46 nm and ν = 0.39, indicating a higher degree of compaction.

We observe that there are no significant changes in the intensity at low Q after cross-linking, indicating that under the conditions employed, the cross-linking is mostly intrachain, and interchain bonding may be considered minor. A slight intensity increase due to the additional molecular weight provided by the cross-linker is expected, but it should be a maximum of a factor of 1.06 for DSG and 1.08 for DSS in case all lysine groups were cross-linked. Thus, the individual BSA chains collapse into unimolecular SCNPs, which demonstrates the success of our approach to synthesize polypeptide SCNPs.

https://doi.org/10.1021/acsomega.2c04805
ACS Omega 2022, 7, 42163−42169

The low-Q upturn in the intensity observed in both curves of BSA and SCNPs in denaturing media is attributed to the denaturing conditions rather than a significant contribution of interchain cross-link formation.

In addition to a size reduction upon cross-linking, the fit of the scattering data using eq 3 revealed a higher scaling exponent, from $\nu = 0.5$ for denatured BSA to $\nu = 0.39$ for the BSA-SCNP synthesized with 28 mol % DSG. To accentuate changes in the macromolecular shape, Figure 3 shows the

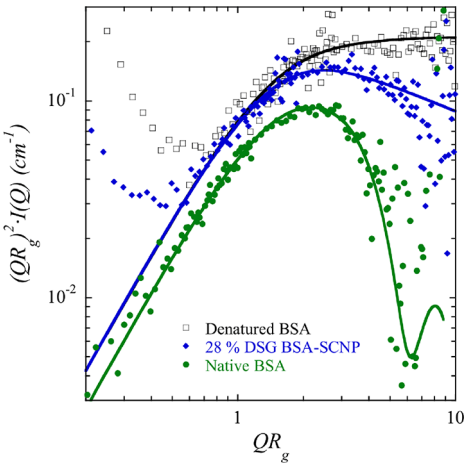

Figure 3. Kratky plot. Continuous lines are fits to a generalized Gaussian coil (see eq 3 in the text) for BSA and BSA-SCNPs in urea (6 M) and a model for an ellipsoid for BSA in its native conformation.

SANS data in a Kratky plot. By rescaling with their respective radii of gyration, we eliminate the size effect and emphasize the differences in the fractal dimension at high Q. We note that differences at very low Q arise as a result of the rescaling with R_g, and we just focus on the high-Q behavior. Comparing the results of the denatured BSA with the SCNPs with 28 mol % DSG, we observe that the data at intermediate Q-values superimpose, whereas differences appear at high Q-values in the range of small length scales due to the internal cross-linking. In denaturing conditions, the scattering intensity of the BSA-SCNPs decays steeper than that of the BSA, revealing a higher degree of compactness, but it does not reach the compaction degree of the BSA in its native state. In this representation, it is clear that the protein denatured with urea (6 M) has a conformation that is roughly a Gaussian random-like walk, as reported in other works,[16,27] rather than a coil in good solvent. This may be attributed to the fact that BSA has intact disulfide cross-links in urea (6 M), which has an impact on the short-length scales of BSA even when denatured as observed by SANS.[27] Moreover, previous SANS experiments have shown that higher concentrations of urea lead to even higher values of R_g due to a higher degree of denaturalization.[16] Here, the R_g value is slightly larger than the one reported for the same urea concentration but lower pH, closer to the isoelectric point of BSA.[16] Thus, taking into account all these arguments, we conclude that the BSA protein is only partially denatured and it compacts more as a consequence of intramolecular cross-linking.

The SANS curves and the fits using the generalized Gaussian coil model for all the synthesized BSA-SCNPs are shown in Figure 4. The fit results are collected in Table 1. In all cases, the cross-linking reaction leads to a progressive size reduction and increased degree of compaction with increasing cross-linker concentration.

Figure 5 shows the radii of gyration obtained for all BSA-SCNPs as a function of the amount and type of cross-linker. The radii of gyration decrease from 7.38 to ca. 5.4 nm upon increasing the cross-linker concentration up to 28 mol % (relative to the total monomer concentration in BSA) according to the progressive collapse of the denatured BSA chain. We also observe from Figure 5 that the longer cross-linker is slightly more efficient in collapsing the polypeptide chain at low contents of cross-linker. The average cross-linker length in its most possible extended conformation can be estimated from the number of carbon bonds to be 0.89 and 0.51 nm for DSS and DSG, respectively. These values were calculated using the program ChemBio3D Ultra simulating the chemical structures in their all-*trans* conformation. Note that they should be taken cautiously because a priori, the actual conformation of the cross-linking segment in the SCNP is

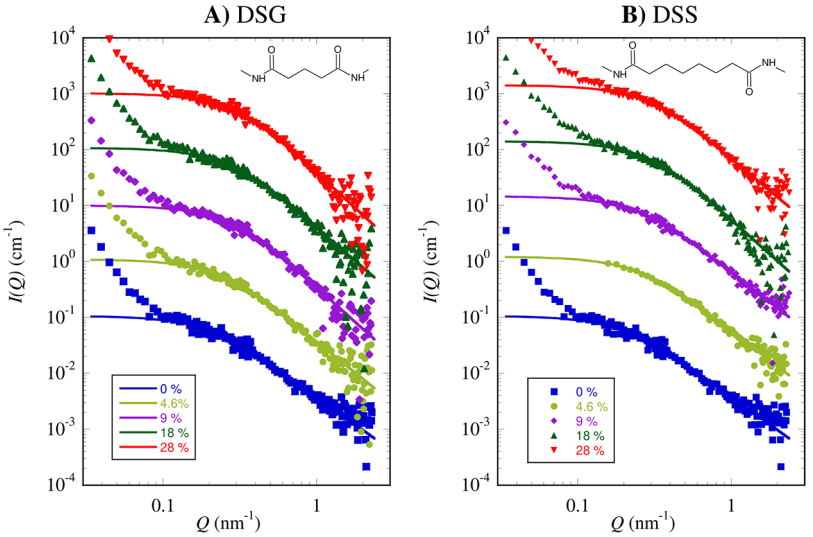

Figure 4. All SANS data of denatured BSA at 1 mg/mL and BSA-SCNPs with (A) DSG and (B) DSS in NaCl (0.6 M)/*d*-urea (6 M)/ D_2O solutions. The curves are shifted vertically for clarity. Lines correspond to the model fit analysis with eq 3 in the main text.

https://doi.org/10.1021/acsomega.2c04805
ACS Omega 2022, 7, 42163−42169

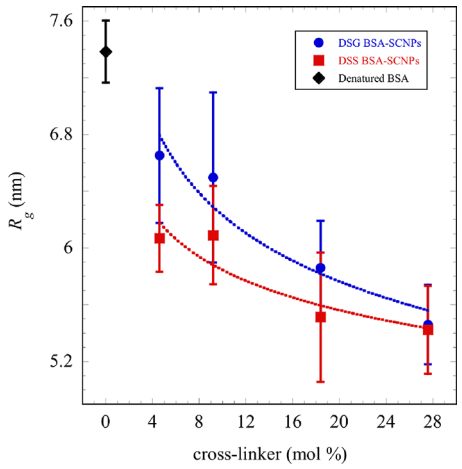

Figure 5. Radii of gyration (R_g) of denatured BSA and BSA-SCNPs synthesized via intrachain cross-linking mediated by DSS or DSG as a function of the added cross-linker concentration. R_g is obtained from fitting a generalized Gaussian coil to the SANS data (eq 3 in the text). Dashed lines are fits to $R_g \approx x^{-y}$ with y=0.11 for DSG and 0.07 for DSS. The error bars represent the maximum width of uncertainty.

unknown. Nevertheless, we can compare them to the size of the denatured BSA—radius of gyration R_g = 7.38 nm and end-to-end distance R_E = 18 nm—and the effective monomer length taking into account the number of amino acids in BSA N = 583, $l = \sqrt{R_E^2/N^{2\nu}}$ = 0.74 nm. The cross-linker lengths seem to be comparable to the effective monomer length. Our SANS results suggest that the longer cross-linker is able to form larger loops, leading to a stronger size reduction. This finding is in agreement with recent literature results, which report that shorter cross-linking molecules have been found to achieve less compaction due to a dominance of short-range loops.[9] The overall size reduction of SCNPs compared to their linear precursors is expected to depend on solvent quality, molecular weight of the precursor, and cross-linking density.[28] Theoretically, the size of elastic single-chain nanoparticles in solution is estimated to scale with the cross-linking density as $R_g \approx x^{-1/5}$ in good solvent and $R_g \approx x^{-1/8}$ in theta solvent.[28,29] Here, in both cases, we obtain lower dependencies, namely, $R_g \approx x^{-0.11}$ and $\approx x^{-0.07}$ for DSG and DSS (dotted lines in Figure 5), respectively, probably due to lower reactivity of the cross-linker added that may yield less effective cross-links or due to the stiffness of the polypeptide chain.

4. CONCLUSIONS

This work provides a straightforward and versatile method to prepare protein-based SCNPs. We have synthesized polypeptide SCNPs based on BSA (bovine serum albumin) denatured with urea (6 M) and cross-linked below the overlap concentration with succinimide-type linkers with two spacer lengths. The degree of cross-linking was estimated by means of ^{1}H NMR, where we found a similar reaction extent for both cross-linkers at a given concentration. The structural changes were probed in the reacting media with SANS. The partially denatured BSA has a random-like conformation and cross-linking leads to "neat" BSA-SCNPs with smaller sizes and more compact structures. As revealed by SANS, the size of the "neat" BSA-SCNPs can be easily tuned by the type and concentration of cross-linker. This method should be applicable to a wide range of proteins since most proteins have lysine-reactive groups and denature in urea, thus paving the way to a new generation of polypeptide SCNPs for nanomedicine.

■ ASSOCIATED CONTENT

Supporting Information

The Supporting Information is available free of charge at https://pubs.acs.org/doi/10.1021/acsomega.2c04805.

Additional ^{1}H-NMR spectra and peak decomposition; additional SANS analysis; complementary SAXS results (PDF)

■ AUTHOR INFORMATION

Corresponding Author

Paula Malo de Molina − *Materials Physics Center (MPC), Centro de Física de Materiales (CFM) (CSIC-UPV/EHU), E-20018 Donostia, Spain; IKERBASQUE—Basque Foundation for Science, E-48009 Bilbao, Spain;* orcid.org/0000-0002-9911-5320; Email: p.malodemolina@ehu.eus

Authors

Thu Phuong Le − *Materials Physics Center (MPC), Centro de Física de Materiales (CFM) (CSIC-UPV/EHU), E-20018 Donostia, Spain*

Amaia Iturrospe − *Materials Physics Center (MPC), Centro de Física de Materiales (CFM) (CSIC-UPV/EHU), E-20018 Donostia, Spain*

Urs Gasser − *Laboratory for Neutron Scattering and Imaging, Paul Scherrer Institut, CH-5232 Villigen, Switzerland*

Arantxa Arbe − *Materials Physics Center (MPC), Centro de Física de Materiales (CFM) (CSIC-UPV/EHU), E-20018 Donostia, Spain;* orcid.org/0000-0002-5137-4649

Juan Colmenero − *Materials Physics Center (MPC), Centro de Física de Materiales (CFM) (CSIC-UPV/EHU), E-20018 Donostia, Spain; Departamento de Polímeros y Materiales Avanzados: Física, Química y Tecnología, University of the Basque Country (UPV/EHU), E-20018 Donostia, Spain; Donostia International Physics Center, E-20018 Donostia, Spain*

José A. Pomposo − *Materials Physics Center (MPC), Centro de Física de Materiales (CFM) (CSIC-UPV/EHU), E-20018 Donostia, Spain; IKERBASQUE—Basque Foundation for Science, E-48009 Bilbao, Spain; Departamento de Polímeros y Materiales Avanzados: Física, Química y Tecnología, University of the Basque Country (UPV/EHU), E-20018 Donostia, Spain*

Complete contact information is available at: https://pubs.acs.org/10.1021/acsomega.2c04805

Notes

The authors declare no competing financial interest.

■ ACKNOWLEDGMENTS

The authors acknowledge the financial support received from the IKUR Strategy under the collaboration agreement between the Ikerbasque Foundation and the Materials Physics Center on behalf of the Department of Education of the Basque Government. Financial support by MCIN/AEI/10.13039/501100011033 and "ERDF − A way of making Europe" (grant PID2021-123438NB-I00), Eusko Jaurlaritza − Basque Government (grant IT-1566-22) and the Gipuzkoako Foru Aldundia, Programa Red Gipuzkoana de Ciencia, Tecnología e

https://doi.org/10.1021/acsomega.2c04805
ACS Omega 2022, 7, 42163−42169

Innovación (2021-CIEN-000010-01) is gratefully acknowledged. A.I. thanks MICINN for a Personal Técnico de Apoyo contract (PTA2017-14359-I).

REFERENCES

(1) Verde-Sesto, E.; Arbe, A.; Moreno, A. J.; Cangialosi, D.; Alegría, A.; Colmenero, J.; Pomposo, J. A. Single-Chain Nanoparticles: Opportunities Provided by Internal and External Confinement. *Mater. Horiz.* **2020**, *7*, 2292−2313.

(2) Arbe, A.; Rubio-Cervilla, J.; Alegría, A.; Moreno, A. J.; Pomposo, J. A.; Robles-Hernández, B.; Malo de Molina, P.; Fouquet, P.; Juranyi, F.; Colmenero, J. Mesoscale Dynamics in Melts of Single-Chain Polymeric Nanoparticles. *Macromolecules* **2019**, *52*, 6935−6942.

(3) Rubio-Cervilla, J.; Malo De Molina, P.; Robles-Hernández, B.; Arbe, A.; Moreno, A. J.; Alegría, A.; Colmenero, J.; Pomposo, J. A. Facile Access to Completely Deuterated Single-Chain Nanoparticles Enabled by Intramolecular Azide Photodecomposition. *Macromol. Rapid Commun.* **2019**, 1900046.

(4) Kröger, A. P. P.; Komil, M. I.; Hamelmann, N. M.; Juan, A.; Stenzel, M. H.; Paulusse, J. M. J. Glucose Single-Chain Polymer Nanoparticles for Cellular Targeting. *ACS Macro Lett.* **2019**, *8*, 95−101.

(5) Hebel, M.; Gačanin, J.; Lückerath, T.; Ng, D. Y. W.; Weil, T. Controlling Polymer Morphologies by Intramolecular and Intermolecular Dynamic Covalent Iron(III)/Catechol Complexation—From Polypeptide Single Chain Nanoparticles to Hydrogels. *Macromol. Rapid Commun.* **2021**, 2100413.

(6) *Single-Chain Polymer Nanoparticles: Synthesis, Characterization, Simulations, and Applications*; Pomposo, J. A., Ed.; Wiley-VCH Verlag GmbH & Co. KGaA: Weinheim, Germany, 2017, DOI: 10.1002/9783527806386.

(7) Lyon, C. K.; Prasher, A.; Hanlon, A. M.; Tuten, B. T.; Tooley, C. A.; Frank, P. G.; Berda, E. B. A Brief User's Guide to Single-Chain Nanoparticles. *Polym. Chem.* **2015**, *6*, 181−197.

(8) Hanlon, A. M.; Martin, I.; Bright, E. R.; Chouinard, J.; Rodriguez, K. J.; Patenotte, G. E.; Berda, E. B. Exploring Structural Effects in Single-Chain "Folding" Mediated by Intramolecular Thermal Diels−Alder Chemistry. *Polym. Chem.* **2017**, *8*, 5120−5128.

(9) Liao, S.; Wei, L.; Abriata, L. A.; Stellacci, F. Control and Characterization of the Compactness of Single-Chain Nanoparticles. *Macromolecules* **2021**, *54*, 11459−11467.

(10) Arbe, A.; Colmenero, J. Structure and Dynamics of Systems Based on Single-Chain Polymer Nano-Particles Investigated by Scattering Techniques. In *Single-Chain Polymer Nanoparticles*; Wiley-VCH Verlag GmbH & Co. KGaA: Weinheim, Germany, 2017; pp. 129−181.

(11) Pomposo, J. A.; Moreno, A. J.; Arbe, A.; Colmenero, J. Local Domain Size in Single-Chain Polymer Nanoparticles. *ACS Omega* **2018**, *3*, 8648−8654.

(12) Moreno, A. J.; Lo Verso, F.; Sanchez-Sanchez, A.; Arbe, A.; Colmenero, J.; Pomposo, J. A. Advantages of Orthogonal Folding of Single Polymer Chains to Soft Nanoparticles. *Macromolecules* **2013**, *46*, 9748−9759.

(13) Lo Verso, F.; Pomposo, J. A.; Colmenero, J.; Moreno, A. J. Multi-Orthogonal Folding of Single Polymer Chains into Soft Nanoparticles. *Soft Matter* **2014**, *10*, 4813−4821.

(14) Moreno, A. J.; Lo Verso, F.; Arbe, A.; Pomposo, J. A.; Colmenero, J. Concentrated Solutions of Single-Chain Nanoparticles: A Simple Model for Intrinsically Disordered Proteins under Crowding Conditions. *J. Phys. Chem. Lett.* **2016**, *7*, 838−844.

(15) Habibi, N.; Mauser, A.; Ko, Y.; Lahann, J. Protein Nanoparticles: Uniting the Power of Proteins with Engineering Design Approaches. *Adv. Sci.* **2022**, *9*, 2104012.

(16) Chodankar, S.; Aswal, V. K.; Kohlbrecher, J.; Vavrin, R.; Wagh, A. G. Structural Evolution during Protein Denaturation as Induced by Different Methods. *Phys. Rev. E* **2008**, *77*, 031901.

(17) Bennion, B. J.; Daggett, V. The Molecular Basis for the Chemical Denaturation of Proteins by Urea. *Proc. Natl. Acad. Sci.* **2003**, *100*, 5142−5147.

(18) Lin, T.; Zhao, P.; Jiang, Y.; Tang, Y.; Jin, H.; Pan, Z.; He, H.; Yang, V. C.; Huang, Y. Blood−Brain-Barrier-Penetrating Albumin Nanoparticles for Biomimetic Drug Delivery via Albumin-Binding Protein Pathways for Antiglioma Therapy. *ACS Nano* **2016**, *10*, 9999−10012.

(19) Stromer, B. S.; Kumar, C. V. White-Emitting Protein Nanoparticles for Cell-Entry and PH Sensing. *Adv. Funct. Mater.* **2017**, *27*, 1603874.

(20) Kohlbrecher, J.; Wagner, W. The New SANS Instrument at the Swiss Spallation Source SINQ. *J. Appl. Crystallogr.* **2000**, *33*, 804−806.

(21) Keiderling, U. The New "BerSANS-PC" Software for Reduction and Treatment of Small Angle Neutron Scattering Data. *Appl. Phys. A: Mater. Sci. Process.* **2002**, *74*, s1455−s1457.

(22) Sadler, P. J.; Tucker, A. Proton NMR Studies of Bovine Serum Albumin. Assignment of Spin Systems. *Eur. J. Biochem.* **1992**, *205*, 631−643.

(23) Mädler, S.; Bich, C.; Touboul, D.; Zenobi, R. Chemical Cross-Linking with NHS Esters: A Systematic Study on Amino Acid Reactivities. *J. Mass Spectrom.* **2009**, *44*, 694−706.

(24) Liu, J. W.; Mackay, M. E.; Duxbury, P. M. Nanoparticle Formation by Crosslinking a Macromolecule. *Europhys. Lett.* **2008**, *84*, 46001.

(25) Zemb, T. Neutrons, X-Rays and Light: Scattering Methods Applied to Soft Condensed Matter. In *Neutrons, X-rays and Light: Scattering Methods Applied to Soft Condensed Matter*; Lindner, P., Zemb, T., Eds.; Elsevier, 2002; p 317.

(26) Hammouda, B. Small-Angle Scattering From Branched Polymers. *Macromol. Theory Simul.* **2012**, *21*, 372−381.

(27) Ameseder, F.; Radulescu, A.; Holderer, O.; Falus, P.; Richter, D.; Stadler, A. M. Relevance of Internal Friction and Structural Constraints for the Dynamics of Denatured Bovine Serum Albumin. *J. Phys. Chem. Lett.* **2018**, *9*, 2469−2473.

(28) De-La-Cuesta, J.; González, E.; Moreno, A. J.; Arbe, A.; Colmenero, J.; Pomposo, J. A. Size of Elastic Single-Chain Nanoparticles in Solution and on Surfaces. *Macromolecules* **2017**, *50*, 6323−6331.

(29) Rabbel, H.; Breier, P.; Sommer, J.-U. Swelling Behavior of Single-Chain Polymer Nanoparticles: Theory and Simulation. *Macromolecules* **2017**, *50*, 7410−7418.

https://doi.org/10.1021/acsomega.2c04805
ACS Omega 2022, 7, 42163−42169